

This is a pre print version of the following article:

Bending of nanobeams in finite elasticity / Lanzoni, Luca; Tarantino, Angelo Marcello. - In: INTERNATIONAL JOURNAL OF MECHANICAL SCIENCES. - ISSN 0020-7403. - 202-203:106500(2021), pp. 1-9.
[10.1016/j.ijmecsci.2021.106500]

Terms of use:

The terms and conditions for the reuse of this version of the manuscript are specified in the publishing policy. For all terms of use and more information see the publisher's website.

05/01/2026 19:12

Nonlinear bending theory of nanobeams

Luca Lanzoni¹, Angelo Marcello Tarantino²

December 29, 2020

¹DIEF, Università di Modena e Reggio Emilia, via P. Vivarelli 10, 41125, Modena, Italy, e-mail: luca.lanzoni@unimore.it,

²DIEF, Università di Modena e Reggio Emilia, via P. Vivarelli 10, 41125, Modena, Italy, e-mail: angelomarcello.tarantino@unimore.it

Abstract

Motivated by the need to have a nonlinear beam model usable at the nanoscale, in this paper, the equilibrium problem of inflexed nanobeams in the context of nonlocal finite elasticity is investigated. Therefore, considering both deformations and displacements large the complete three-dimensional kinematics of an inflexed nanobeam is derived on the basis of classic assumption that cross sections maintain their planarity (Bernoulli Navier hypothesis). Extending the Eringen theory, a constitutive law in integral form for the nonlocal tensor of Cauchy stresses has been then proposed. Finally, by imposing the equilibrium conditions, the governing equations are obtained. These take the form of a coupled system of three equations in integral form, which is solved numerically. Explicit formulae for displacements, stretches and stresses in every point of the nanobeam are derived. By way of example, a simply supported nanobeam has been considered. The shapes assumed by the inflexed nanobeam, as the internal characteristic length varies, are shown through some graphs. The results obtained have been discussed and compared with those provided by the local theory.

Keywords: Finite elasticity; Hyperelasticity; Equilibrium; Nanobeam; Bending moment, Nonlocal effect.

1 Introduction

Nanobeams are fundamental mechanical components in different areas of modern nanotechnology. In particular, they have broad applications such as nano-sensors and nano-actuators in micro-electromechanical systems (MEMS) and nano-electromechanical systems (NEMS).

As is well known, classical local continuum mechanics is not appropriate for studying nanobeams since it fails to capture the size-dependent effects. Atomistic and molecular mechanics are certainly valid for investigating the mechanical behavior at small length scales, however, they are difficult to apply accurately and are computationally burdensome. Nonlocal continuous models, on the other hand, represent effective attempts to investigate nanobeams, as they retain many advantages of the theory in modeling and numerical computations.

First studies in this direction date back to Kröner [1] and Krumhansl [2]. Other contributions on nonlocal continuum mechanics were proposed later by Edelen and Laws [3], Edelen, Green and Laws [4], Eringen and Edelen [5], Eringen and Kim [6] and Eringen [7]. In particular, Eringen [8] recognized that an internal characteristic length is necessary in the modeling of physical problems when the influence of microstructural effects is significant. Peddieson, Buchanan and McNitt [9] were the first to apply nonlocal continuum mechanics to capture the size effects on bending of cantilever nanobeams. Recent contributions on this subject can be found in [10], [11], [12], [13] and [14].

The scientific literature reports many practical situations in which nanobeams are strongly flexed, experiencing large displacements. For example, a series of electric sensors for large bending deformation has recently been applied to human motion monitoring and human-machine interaction [15], [16]. These sensors provide some advantages such as extreme durability and high reproducibility [17]. Piezoelectric actuators are used for their excellent guiding accuracy during bending of beams. When a flat piezo contracting actuator is coupled to a substrate, the driving and contraction of the ceramic creates a bending moment, which converts the small change in length into a large vertical displacement [18]. Large bending actuators are also made using shape memory alloys (SMA). In this case, a contractile wire, usually in nickel-titanium, is applied on the surface of a flexible beam or strip. The SMA wire is connected to both ends of the beam, so that a small change in the strain of the SMA wire results in a large bending deformation of the beam [19]. There is a growing interest in the flexoelectric effect, since experimental results shown large flexoelectric bending [20], [21], [22] and [23]. In particular, a direct observation of extraordinarily large and reversible bending in dysprosium scandate is reported in [24]. Similar results hold for terbium and gadolinium scandate.

Despite the numerous applications in emerging scientific fields, where the nonlinear effects related to large deformations and large displacements are evident, to date a modeling of nanobeams in the framework of fully nonlinear continuum mechanics is still not available. The present paper is conceived to remove this gap.

The paper is organized as follows. Considering slender nanobeams with compact cross section, a three-dimensional kinematic model based on the classic hypothesis that cross sections deform preserving their planarity has been developed in Section 2. Both strains and displacements are considered large and the anticlastic deformation of the cross sections has been also taken into account. Extending the nonlocal linear elasticity to the more general context of the finite elasticity, the nonlocal Cauchy stress tensor has been defined in

Section 3 through an integral constitutive model. Subsequently, by imposing the equilibrium conditions, the governing equations are obtained. These take the form of a coupled system of three equations in integral form, which is solved numerically. Solving this system, the displacement field, the shape assumed by the nanobeam in the deformed configuration, as well as stretches and stresses in every point of the nanobeam, can be assessed. All the mathematical formulation was performed for a generic hyperelastic and isotropic material. In view of the applications, the analysis was then specialized for compressible Mooney-Rivlin materials in Section 4. By way of example, a simply supported nanobeam has been considered. For this simple structural system, the shapes assumed by inflexed nanobeam, as the internal characteristic length varies, are computed and displayed through some graphs. The results obtained using the nonlocal theory have been finally compared and discussed with those provided by the classical local theory.

2 Kinematics

Let us consider a hyperelastic body composed of a homogeneous, isotropic and compressible material¹ having the shape of a rectangular parallelepiped. Reference is made to a Cartesian coordinate system $\{O, X, Y, Z\}$, with the origin O placed in the centroid of the end cross section, as shown in Fig. 1a. Thus, the body can be identified with the closure of the following regular region:

$$\mathcal{B} = \left\{ (X, Y, Z) \mid -\frac{B}{2} < X < \frac{B}{2}, -\frac{H}{2} < Y < \frac{H}{2}, 0 < Z < L \right\},$$

of the three-dimensional Euclidean space \mathcal{E} . The symbols B , H and L respectively denote the width, height and length of the body. As is typical in the case of beams, the length L is predominant on the both transverse dimensions B and H . As shown in Fig. 1, three-dimensional beams vertically inflexed are considered. Although the formulation is presented for beams with a rectangular cross section, it can readily be extended to beams with a generic cross section provided that the symmetry with respect to Y axis is maintained.

The undeformed configuration $\bar{\mathcal{B}}$ of the beam is assumed as the reference configuration, whereas the deformed configuration is given by the *deformation* $\mathbf{f}: \bar{\mathcal{B}} \rightarrow \mathcal{V}$,² that is a smooth enough, injective and orientation-preserving vector field (in the sense that $\det \mathbf{D}\mathbf{f} > 0$). The deformation of a generic material point P belonging to $\bar{\mathcal{B}}$ can be expressed by the well-known relationship

$$\mathbf{f}(P) = \mathbf{s}(P) + \mathbf{id}(P), \quad (1)$$

where $\mathbf{id}(P)$ and

$$\mathbf{s}(P) = u(P)\mathbf{i} + v(P)\mathbf{j} + w(P)\mathbf{k} \quad (2)$$

¹It should be kept in mind that the internal constraint of incompressibility, especially in the case of large deformations, can significantly affect the shape assumed by an inflexed body [25], [26].

² \mathcal{V} is the vector space associated with the Euclidean space \mathcal{E} .

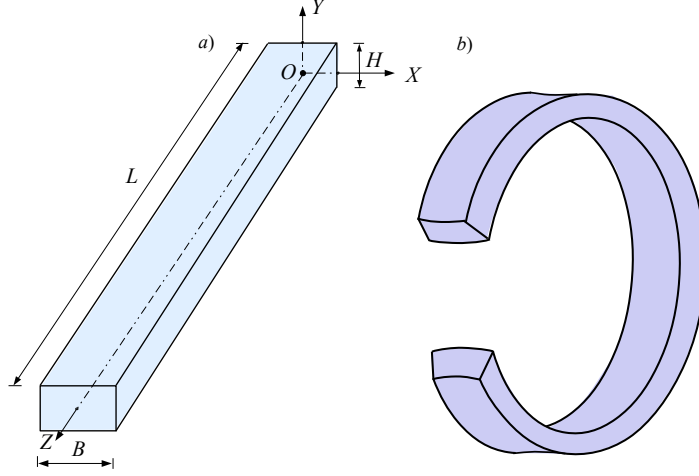


Figure 1: Prismatic slender beam $\bar{\mathcal{B}}$. (a) Undeformed configuration. (b) Deformed configuration.

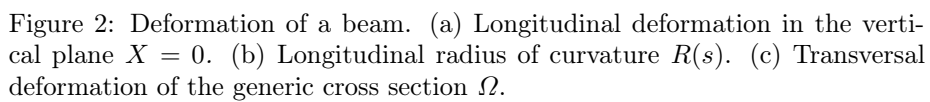
are the position and displacement vectors of the point P . In the vectorial equation (2), functions $u(P)$, $v(P)$ and $w(P)$ are the scalar components of $\mathbf{s}(P)$, whereas \mathbf{i} , \mathbf{j} and \mathbf{k} are the unit vectors. In the sequel, an Eulerian coordinate system $\{O, x, y, z\}$ is also used (cf. Fig. 2). Points and other geometric objects belonging to the deformed configuration are indicated with an apex, $(\cdot)'$.

To derive the displacement field of an inflexed beam under variable curvature a semi-inverse approach, which involves the definition of a kinematic model, is followed. This model is based on the following three basic hypotheses:

1. In the bending of the beam, cross sections maintain their planarity (*Bernoulli-Navier hypothesis*). That is, plane cross sections, orthogonal to Z axis, remain as such after the beam has been inflexed.
2. Due to the longitudinal inflexion also cross sections are transversely inflexed, but with opposite curvature (*anticlastic effect*). This transversal inflexion is assumed to occur with constant curvature (cf. Fig. 2c).
3. Slender beams with compact cross sections are considered.

The first assumption, which is very popular in the linear mechanics of beams under pure bending, predicts the conservation of the planarity of cross sections after the deformation. For beams that satisfy the third assumption, the reliability of such hypothesis in nonlinear theory has recently been checked both from the experimental and numerical points of view in [25], [27] and [28]. The second hypothesis also becomes acceptable when beams satisfy the third hypothesis [25].

Suppose that the previous hypotheses, formulated in the bending theory of beams (see [25], [29]) are substantially valid for the bending theory of nanobeams,



which will be developed in the next Section.

We then begin to study the equilibrium problem of inflexed nanobeams by examining the kinematic aspects. Based on the three previous hypotheses, the displacement field will be derived as the outcome of the coupled effects generated by both longitudinal and transversal curvatures. The beam axis

$$\mathcal{L} = \{(X, Y, Z) \mid X = Y = 0, Z = Z\},$$

which collects all centroids of the cross sections, is vertically inflexed with variable curvature, so it is transformed into a generic smooth plane curve. Points of the deformed beam axis $N' \in \mathcal{L}'$ are images of points $N \in \mathcal{L}$, that is of points belonging to the horizontal rectilinear segment traced for the point O of the undeformed configuration. Just for convenience, the point O may be considered fixed, $O = O'$ and $\theta_X(0, 0, 0) = 0$ (*cf.* Fig. 2). In this way the global rigid displacements are eliminated.³

By virtue of the first hypothesis, each cross section

$$\Omega = \left\{ (X, Y, Z) \mid -\frac{B}{2} < X < \frac{B}{2}, -\frac{H}{2} < Y < \frac{H}{2}, Z = Z \right\}$$

moves rigidly, remaining plane and orthogonal to the deformed nanobeam axis. At the same time, this cross section deforms in its own plane. Therefore, to define the kinematics of a generic cross section Ω four functions are required. Three functions are necessary to evaluate the rigid displacement of the cross section: $v(0, 0, Z)$, $w(0, 0, Z)$ and $\theta_X(0, 0, Z)$. The first two functions are the displacement components of the centroid of the cross section, while the third represents its rotation around the X axis (*cf.* Fig. 2c). Given the second hypothesis, the cross section is inflexed in its own plane with constant curvature. The radius of curvature $r(0, 0, Z)$ of the transversal basic line is the fourth unknown function (*cf.* Fig. 2c).

Based on the hypotheses formulated for the kinematic model, the displacement field for a three-dimensional beam inflexed vertically with variable curvature is [25], [29]

$$\begin{cases} u = -X + r(Z) e^{-\frac{Y}{r(Z)}} \sin \frac{X}{r(Z)} \\ v = v_N(Z) - Y + r(Z) \left[1 - e^{-\frac{Y}{r(Z)}} \cos \frac{X}{r(Z)} \right] \cos \theta_N(Z) \\ w = w_N(Z) + r(Z) \left[1 - e^{-\frac{Y}{r(Z)}} \cos \frac{X}{r(Z)} \right] \sin \theta_N(Z), \end{cases} \quad (3)$$

where $v_N(Z) = v(0, 0, Z)$, $w_N(Z) = w(0, 0, Z)$ and $\theta_N(Z) = \theta_X(0, 0, Z)$. The function $r(Z)$ denotes the anticlastic radius (*cf.* Fig. 2c).

From system (3), the principal stretches λ_X , λ_Y and λ_Z are derived [25], [29]

$$\begin{cases} \lambda_X = \lambda_Y = e^{-\frac{Y}{r(Z)}} \\ \lambda_Z = 1 + \frac{r(Z)}{R(Z)} \left[1 - e^{-\frac{Y}{r(Z)}} \cos \frac{X}{r(Z)} \right], \end{cases} \quad (4)$$

³These are the constraint conditions of the cantilever beam illustrated in Fig. 2. Obviously other constraints can be used to prevent the rigid global displacements.

where $R(Z)$ denotes the longitudinal radius of curvature of the beam axis (cf. Fig. 2b) and its inverse is given by the following derivative:

$$\frac{d\theta_N}{dZ} = \frac{1}{R(Z)}. \quad (5)$$

As shown in [25], in the case of slender beams, the beam axis does not undergo variations in length ($\lambda_Z = 1$). Thus, although the beam is not, its axis can be considered inextensible. Consequently, $Z = s$, where s is the curvilinear abscissa measured in the deformed configuration (cf. Fig. 2a). Therefore, in terms of Eulerian variables the stretches (4) can be rewritten with the following simple and compact formulae:

$$\begin{cases} \lambda_x = \lambda_y = 1 - \frac{\tilde{y}}{r(s)} \\ \lambda_z = 1 + \frac{\tilde{y}}{R(s)}, \end{cases} \quad (6)$$

where

$$\tilde{y} = \frac{y - v_N(s)}{\cos \theta_N(s)}, \quad \hat{y} = \frac{1}{\cos \beta(s)} [\tilde{y} - r(s)(1 - \cos \beta(s))], \quad (7)$$

with $\beta(s) = \frac{X}{r(s)} = \arctan \left(\frac{x}{r(s) - \frac{y - v_N(s)}{\cos \theta_N(s)}} \right)$. The geometric meanings of the \tilde{y} and \hat{y} ordinates are shown in Fig. 3. It is important to note that the linear law obtained for the stretch λ_z and the rectilinear shape of the neutral axis (line of spatial points for which $\lambda_z = 1$) are direct consequences of the kinematic model adopted. In fact, given the hypothesis of the planarity preservation for cross sections, all cross sections deform maintaining own plane and rotating around the neutral axis of the finite angle $\theta_N(s)$. This kind of deformation leads directly to expression (6)₂ for the longitudinal stretch λ_z in the spatial configuration.

The application of the material gradient to (1) gives

$$\mathbf{F} = \mathbf{H} + \mathbf{I}, \quad (8)$$

where $\mathbf{F} : \bar{\mathcal{B}} \rightarrow Lin^+$ and $\mathbf{H} : \bar{\mathcal{B}} \rightarrow Lin$ ⁽⁴⁾ are the deformation and displacement gradients, respectively. \mathbf{I} is the identity tensor. Using (3) and (4), the components of the deformation gradient \mathbf{F} can be expressed as

$$[\mathbf{F}] = \begin{bmatrix} \lambda_X \cos \beta(s) & -\lambda_Y \sin \beta(s) & 0 \\ \lambda_X \sin \beta(s) \cos \theta_N(s) & \lambda_Y \cos \beta(s) \cos \theta_N(s) & -\lambda_Z \sin \theta_N(s) \\ \lambda_X \sin \beta(s) \sin \theta_N(s) & \lambda_Y \cos \beta(s) \sin \theta_N(s) & \lambda_Z \cos \theta_N(s) \end{bmatrix}. \quad (9)$$

Given the polar decomposition theorem, $\mathbf{F} = \mathbf{R}\mathbf{U}$, it is immediate to write the deformation gradient (9) as product of the rotation tensor \mathbf{R} by the stretch tensor \mathbf{U} , where⁵

$$[\mathbf{R}] = \begin{bmatrix} \cos \beta(s) & -\sin \beta(s) & 0 \\ \sin \beta(s) \cos \theta_N(s) & \cos \beta(s) \cos \theta_N(s) & -\sin \theta_N(s) \\ \sin \beta(s) \sin \theta_N(s) & \cos \beta(s) \sin \theta_N(s) & \cos \theta_N(s) \end{bmatrix} \quad (10)$$

⁴ Lin is the set of all (second order) tensors whereas Lin^+ is the subset of tensors with positive determinant.

⁵ \mathbf{R} is a proper orthogonal tensor, $\mathbf{Q}^T = \mathbf{Q}^{-1}$, with $\det \mathbf{Q} = 1$. \mathbf{U} is a positive definite and symmetric tensor, $\mathbf{U}\mathbf{n} \cdot \mathbf{n} > 0$ for $\forall \mathbf{n} - \{\mathbf{o}\}$ and $\mathbf{U} = \mathbf{U}^T$.

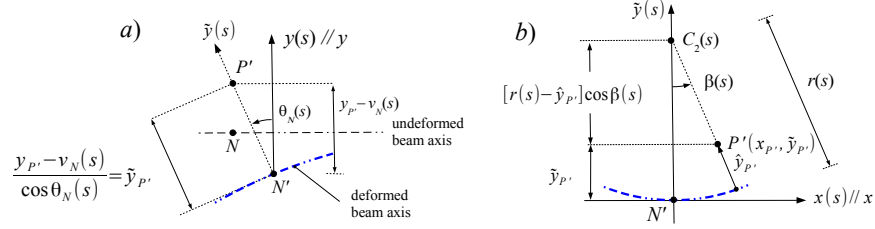


Figure 3: Variables \tilde{y} and \hat{y} of the Eulerian stretches. (a) Longitudinal ordinate \tilde{y} . (b) Transversal ordinate \hat{y} .

and

$$[\mathbf{U}] = \begin{bmatrix} \lambda_X & 0 & 0 \\ 0 & \lambda_Y & 0 \\ 0 & 0 & \lambda_Z \end{bmatrix}. \quad (11)$$

On the basis of the hypotheses formulated for the kinematic model, the deformation gradient (9) describes the deformation state of each single point of the nanobeam. The rotation tensor (10) highlights that each point undergoes a longitudinal rotation $\theta_N(s)$, which is the same for the entire cross section, and a transversal rotation $\beta(s)$, within the cross section (cf. Fig. 2c). The stretch tensor (11) characterizes the pure deformations. It is diagonal because the reference system $\{O, X, Y, Z\}$ is principal for the deformation state derived from (3).

As already mentioned, the nonlinear displacement and deformation fields, illustrated in this Section, have four unknown functions: The three functions related to the deformed axis of the nanobeam, $v_N(s)$, $w_N(s)$ and $\theta_N(s)$, and the anticlastic radius, $r(s)$. These four functions are determined by imposing equilibrium conditions.

Constitutive properties of a hyperelastic material are described by the stored energy function ω . If the function ω is frame-indifferent, homogeneous and isotropic, then it depends only on the principal invariants I_i , with $i = 1, 2$ and 3, of the left Cauchy-Green strain tensor $\mathbf{B} = \mathbf{F}\mathbf{F}^T$ (which coincide with those of the right Cauchy-Green strain tensor $\mathbf{C} = \mathbf{F}^T\mathbf{F}$)⁶

$$\begin{aligned} I_1 &= \|\mathbf{F}\|^2 = \lambda_X^2 + \lambda_Y^2 + \lambda_Z^2, \\ I_2 &= \|\mathbf{F}^*\|^2 = \lambda_X^2 \lambda_Y^2 + \lambda_X^2 \lambda_Z^2 + \lambda_Y^2 \lambda_Z^2, \\ I_3 &= (\det \mathbf{F})^2 = \lambda_X^2 \lambda_Y^2 \lambda_Z^2. \end{aligned}$$

After having introduced these assumptions, the constitutive law ($\mathbf{T}_R = \partial\omega/\partial\mathbf{F}$) takes the following form:

⁶The following notations: $\|\mathbf{A}\| = (\text{tr} \mathbf{A}^T \mathbf{A})^{1/2}$ for the tensor norm in the linear tensor space Lin and $\mathbf{A}^* = (\det \mathbf{A}) \mathbf{A}^{-T}$ for the cofactor of tensor \mathbf{A} (if \mathbf{A} is invertible) are used.

$$\mathbf{T}_R = 2 \left(\frac{\partial \omega}{\partial I_1} + I_1 \frac{\partial \omega}{\partial I_2} \right) \mathbf{F} - 2 \frac{\partial \omega}{\partial I_2} \mathbf{B} \mathbf{F} + 2 I_3 \frac{\partial \omega}{\partial I_3} \mathbf{F}^{-T}, \quad (12)$$

where the tensor \mathbf{T}_R denotes the (first) Piola-Kirchhoff stress tensor.

Being $\mathbf{B} \mathbf{F} = \mathbf{R} \mathbf{U}^3$ and $\mathbf{F}^{-T} = \mathbf{R} \mathbf{U}^{-1}$, the tensorial equation (12) can be rewritten as

$$\mathbf{T}_R = \mathbf{R} \mathbf{S}. \quad (13)$$

From the kinematic model described above, the tensors \mathbf{R} and \mathbf{U} are known (see (10) and (11)). Being the tensor \mathbf{U} diagonal also the tensor \mathbf{S} in (13) is such

$$[\mathbf{S}] = \begin{bmatrix} S_X & 0 & 0 \\ 0 & S_Y & 0 \\ 0 & 0 & S_Z \end{bmatrix},$$

with

$$S_J = 2 \left(\frac{\partial \omega}{\partial I_1} + I_1 \frac{\partial \omega}{\partial I_2} \right) \lambda_J - 2 \frac{\partial \omega}{\partial I_2} \lambda_J^3 + 2 I_3 \frac{\partial \omega}{\partial I_3} \frac{1}{\lambda_J}, \quad \text{for } J = X, Y, Z.$$

Lagrangian stresses were expressed by the Piola-Kirchhoff stress tensor \mathbf{T}_R , while the stress measure coherently employed in the spatial configuration is that of Cauchy. The Cauchy stress tensor \mathbf{T} is obtained from the Piola-Kirchhoff stress tensor \mathbf{T}_R through the well-known transformation

$$\mathbf{T}_R = \mathbf{T} \mathbf{F}^*, \quad (14)$$

which given (9), (10), (11) and (13) provides the following components of the Cauchy stress tensor ($S = S_X = S_Y$, $\lambda = \lambda_X = \lambda_Y$):

$$(\lambda^2 \lambda_Z) [\mathbf{T}] = \begin{bmatrix} S \lambda & 0 & 0 \\ 0 & S \lambda \cos^2 \theta_N(s) + S_Z \lambda_Z \sin^2 \theta_N(s) & (S \lambda - S_Z \lambda_Z) \sin \theta_N(s) \cos \theta_N(s) \\ 0 & (S \lambda - S_Z \lambda_Z) \sin \theta_N(s) \cos \theta_N(s) & S \lambda \sin^2 \theta_N(s) + S_Z \lambda_Z \cos^2 \theta_N(s) \end{bmatrix}, \quad (15)$$

being $\mathbf{F}^* = (\lambda^2 \lambda_Z) \mathbf{R} \mathbf{U}^{-1}$ and $(\lambda^2 \lambda_Z) \mathbf{T} = \mathbf{R} \mathbf{S} \mathbf{U} \mathbf{R}^T$. The tensor \mathbf{T} is symmetric. The matrix (15) can be rewritten in diagonal form by evaluating its eigenvalues. The resolution of the characteristic polynomial allows the determination of the principal Cauchy stresses

$$[\mathbf{T}] = \begin{bmatrix} \frac{S}{\lambda \lambda_Z} & 0 & 0 \\ 0 & \frac{S}{\lambda \lambda_Z} & 0 \\ 0 & 0 & \frac{S_Z}{\lambda_Z^2} \end{bmatrix}, \quad (16)$$

where

$$T_1 = T_2 = \frac{S}{\lambda \lambda_Z} = \frac{2}{\lambda_Z} [\omega_1 + (\lambda^2 + \lambda_Z^2) \omega_2 + \lambda^2 \lambda_Z^2 \omega_3], \quad (17)$$

$$T_3 = \frac{S_Z}{\lambda^2} = \frac{2}{\lambda^2} [\lambda_Z \omega_1 + 2\lambda^2 \lambda_Z \omega_2 + \lambda^4 \lambda_Z \omega_3].$$

Since Cauchy stresses are Eulerian functions, in the above formulae it is more appropriate to use stretches with the equivalent Eulerian form (6). The principal directions of stress are the eigenvectors associated with these eigenvalues. The principal direction corresponding to the eigenvalue T_3 is the unit vector orthogonal to the plane Ω' (*cf.* Fig. 2c) with components $(0, -\sin \theta_N(s), \cos \theta_N(s))$. The others two eigenvectors are any two unit vectors orthogonal to each other and belonging to the plane Ω' .

Finally, it is recalled that by imposing the equilibrium equations for the points belonging to the beam axis, the following relationship, which connects the anticlastic radius $r(s)$ with the longitudinal one $R(s)$, is obtained [25], [29]:

$$-\frac{2}{r(s)} \omega_1 + 2\omega_{1,Y} + \left[\frac{4}{R(s)} - \frac{8}{r(s)} \right] \omega_2 + 4\omega_{2,Y} + \left[\frac{4}{R(s)} - \frac{6}{r(s)} \right] \omega_3 + 2\omega_{3,Y} = 0, \quad (18)$$

where $\omega_{i,K} = \frac{\partial}{\partial K} \left(\frac{\partial \omega}{\partial I_i} \right)$ for $i = 1, 2, 3$ and $K = X, Y$.

Using the results described above, in the next Section, the equilibrium problem for inflexed nanobeams is formulated.

3 Nonlocal constitutive law and equilibrium

As proposed by Eringen, to construct a nonlocal theory it is sufficient to change the constitutive relationship, leaving compatibility and equilibrium equations formally unmodified [30]. Extending the nonlocal linear elasticity, the nonlocal Cauchy stress tensor, $\mathbf{T}^{nl}(P')$, in a generic point P' of the deformed configuration, can be defined by the following integral constitutive model:⁷

$$\mathbf{T}^{nl}(P') = \int_{B'} \phi(|P' - Q'|; \varrho) \mathbf{T}(Q') dv(Q'). \quad (19)$$

With (19), the nonlocal stress is expressed as a convolution law that depends on the kernel $\phi(|P' - Q'|; \varrho)$. This kernel governs the attenuation of the nonlocal interactions with the distance $|P' - Q'|$. In the kernel expression there is the nonlocal parameter $\varrho > 0$. Through this parameter it is possible to assess the internal characteristic length $L_c = \varrho L$, which measures the extent of the nonlocality effect. As $L_c \rightarrow 0$, ϕ converges to the Dirac delta function $\delta(P')$, so that from (19) the classical local stress is recovered. The kernel ϕ is positive, symmetric and takes its maximum $\phi(0; \varrho)$ at $P' = Q'$ and decreases (usually fairly quickly) when Q' moves away from P' . Furthermore, in the case of unlimited

⁷Writing the constitutive law directly in terms of Cauchy stress, that is, in terms of actual stress, appears more consistent with physical reality. After all, the use of Piola-Kirchhoff stress produces theoretical incongruences, such as a consequent non-symmetric Cauchy stress tensor.

domain, the kernel ϕ satisfies the following normalization condition:

$$\int_{-\infty}^{\infty} \phi(|P' - Q'|; \varrho) dv(Q') = 1. \quad (20)$$

By attributing to kernel ϕ the meaning of a probability density function, the comparison of (19) with (20) shows that the nonlocal Cauchy stress at the generic point P' can be considered as an average of local stresses related to all points Q' of the deformed body. Based on these considerations, Eringen [31] proposed the following expression for the kernel ϕ of the Green's function type:

$$\phi(|P' - Q'|; \varrho) = \frac{1}{2L_c} e^{(-\frac{|P' - Q'|}{L_c})}. \quad (21)$$

As is usual for nanobeams, the nonlocal effect is considered only longitudinally [12]. Therefore, taking into account (21), (19) is simplified in

$$\mathbf{T}^{\text{nl}}(x, y, z) = \frac{1}{2L_c} \int_0^{L'} e^{(-\frac{|z - \xi|}{L_c})} \mathbf{T}(x, y, \xi) d\xi, \quad (22)$$

that is, a nonlocal stress component at the z coordinate is determined by calculating the integral (22), which involves all corresponding local component stresses along the nanobeam.

By introducing the local stress component T_3 in (22), the corresponding nonlocal component T_3^{nl} can be evaluated. Next, the internal bending moment for each deformed cross section Ω' of the nanobeam can be calculated by integrating the elementary moments generated by the principal nonlocal Cauchy stress T_3^{nl} orthogonal to Ω' . Thus, using the polar coordinate (ρ, β) with pole at the point $C_2(s)$ of Fig. 2c, the moment $m_x^{\text{int}}(s)$ can be computed by the following integral:

$$m_x^{\text{int}}(s) = \int_{-\beta_0(s)}^{\beta_0(s)} \int_{\rho_{\min}(s)}^{\rho_{\max}(s)} \rho T_3^{\text{nl}}(\rho, \beta) \tilde{y}(s) d\rho d\beta, \quad (23)$$

where $\tilde{x}(s) = \rho \sin \beta$, $\tilde{y}(s) = r(s) - \rho \cos \beta$, and

$$\begin{aligned} \rho_{\min}(s) &= r(s) - \int_0^{\frac{H}{2}} \lambda_Y(\hat{Y}) d\hat{Y} = r(s) e^{-\frac{H}{2r(s)}}, \\ \rho_{\max}(s) &= r(s) + \int_{\frac{H}{2}}^0 \lambda_Y(\hat{Y}) d\hat{Y} = r(s) e^{\frac{H}{2r(s)}}. \end{aligned}$$

Due to (17)₂ and (22), the internal moment (23) depends on the unknown radii $R(s)$ and $r(s)$, which are linked by formula (18). Moreover, the internal moment

is evaluated with respect to the deformed axis of the nanobeam which is not known *a priori*.

For equilibrium, the internal bending moment (23) must equal the external bending moment $m_x^{ext}(s)$ produced by external loads in correspondence of the same cross section Ω'

$$m_x^{int}(s) = m_x^{ext}(s), \quad (24)$$

with $s \in \mathcal{L}'$. We will refer to this equation as the moment-curvature relationship in the general form. In fact it, derived in the fully nonlinear context of finite elasticity, relates the bending moment $m_x^{ext}(s)$ with the curvature $R(s)^{-1}$, both evaluated along the deformed nanobeam axis. Through (5), the curvature in (24) can be expressed in geometrically exact manner by the derivative of the rotation $\theta_N(s)$.

The position occupied by the nanobeam axis in the deformed configuration is determined by calculating the two displacement components $v_N(s)$ and $w_N(s)$. These components can be expressed in terms of rotation $\theta_N(s)$

$$\begin{aligned} v_N(s) &= v_N(0) - \int_{0^+}^s \sin \theta_N(\zeta) d\zeta, \\ w_N(s) &= w_N(0) - \int_{0^+}^s (1 - \cos \theta_N(\zeta)) d\zeta. \end{aligned} \quad (25)$$

The above equations in integral form are obtained by integrating the following infinitesimal displacements: $dv_N = -\sin \theta_N ds$, $dw_N = -(1 - \cos \theta_N) ds$, generated by the rotation of an infinitesimal and inextensible horizontal element.

The three equations (24) and (25), supported by equations (5) and (18), constitute a coupled and nonlinear system for computing the displacements and rotations of the nanobeam axis, $v_N(s)$, $w_N(s)$ and $\theta_N(s)$, as well as the radii $R(s)$ and $r(s)$. Such a system can be solved through the iterative numerical procedure illustrated in Appendix A of [29]. With this procedure, typical for solving nonlinear systems, the kinematic functions $v_N(s)$, $w_N(s)$, $\theta_N(s)$, $R(s)$ and $r(s)$ are gradually updated until all governing equations converge. Knowing these kinematic functions, equations (3) and (1) give the displacement field and the three-dimensional shape assumed by the nanobeam in the deformed configuration. During the iterative procedure, stretches and stresses for each point of the nanobeam in the current configuration are evaluated using (6) and (22). By means of the procedure just described the nonlocal solution is achieved. However, the numerical iterative procedure must be applied twice. A first application is in fact necessary to evaluate the corresponding local solution ($\varrho = 0$), which is obtained by introducing in the expression of the internal bending moment (23) the local stress component T_3 instead of the nonlocal component T_3^{nl} and not changing the other equations. Once the component T_3 has been calculated for each point of the nanobeam the corresponding nonlocal components T_3^{nl} can be obtained through (22) and then the execution of the

second iterative procedure can begin. In the latter, the local solution is used as a first attempt solution.

4 Application to compressible Mooney-Rivlin materials

The stored energy function of a compressible Mooney-Rivlin material has the following form:^{8, 9}

$$\omega(I_1, I_2, I_3) = aI_1 + bI_2 + \Gamma(\delta). \quad (26)$$

The function $\Gamma(\lambda_1\lambda_2\lambda_3)$, with $\lambda_1\lambda_2\lambda_3 = \det \mathbf{F} = I_3^{1/2} = \delta$, is convex and satisfies the growth conditions both as $\delta \rightarrow 0^+$ and $\delta \rightarrow \infty$. Hereinafter the expression proposed by Ciarlet and Geymonat [37] is chosen for the function $\Gamma(\delta)$

$$\Gamma(\delta) = c\delta^2 - d \ln \delta, \quad (27)$$

where c and d are positive constants.

With (26), the following derivatives are computed ($\lambda_1 = \lambda_2 = \lambda$):

$$\omega_1 = a, \quad \omega_2 = b, \quad \omega_3 = c - \frac{d}{2\lambda^4\lambda_3^2}. \quad (28)$$

By introducing (28) in (13), Piola-Kirchhoff stresses can be calculated for each point of the beam.

A relationship among the constitutive constants involved in (26) can be established by imposing that, in the absence of deformation, the stress vanishes. By setting $\beta(s) = \theta_N(s) = 0$ into (13), the stresses $T_{R,ij}$, with $i \neq j$, for $i, j = 1, 2, 3$, are zero, whereas the diagonal component for $\lambda_i = 1$ are

$$T_{R,11} = T_{R,22} = T_{R,33} = 2(\omega_1 + 2\omega_2 + \omega_3) |_{\lambda_i=1} = 0. \quad (29)$$

By inserting in this condition the derivatives (28), written for $\lambda_i = 1$, the following relationship for the evaluation of the constant d is obtained:¹⁰

$$d = 2(a + 2b + c), \quad (30)$$

Using this expression, along the nanobeam axis, it occurs that $S_X = S_Y = S_Z = 0$.

Using (4), (28) and (30), equation (18) becomes

$$r(s) = \frac{a + 3b + 2c}{b + c} R(s). \quad (31)$$

⁸The compressible Mooney-Rivlin stored energy function was used, for example, in [34], [35] and [36].

⁹To use the repeated index convention in the following the subscripts X , Y and Z are replaced with the numbers 1, 2 and 3, respectively.

¹⁰A similar position has been used, for example, in [38], [39] and [40].

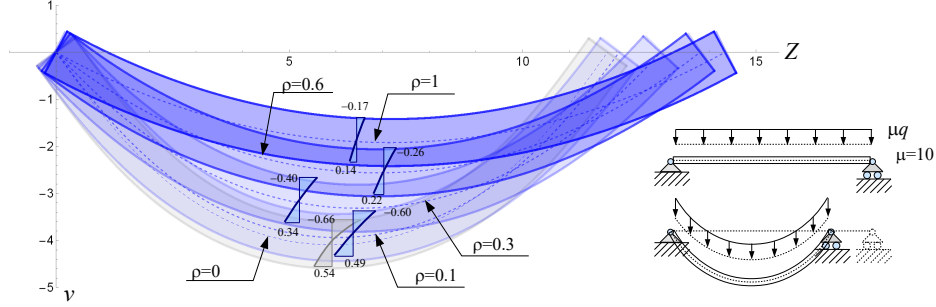


Figure 4: Simply supported nanobeam under uniformly distributed vertical dead loads μq . Deflection curves as the nonlocal parameter ϱ varies.

All applications are performed for the same nanobeam with the following geometrical and constitutive dimensionless parameters: $H = 1$, $B = 2$, $L = 15$, $a = 1$, $b = 0.05$, $c = 2.256$. The numerical values of the constitutive parameters are related to a neoprene [26] and [29]. Let's consider the simply supported beam subjected to the uniformly distributed dead load μq as shown in Fig. 4. The base value of the external load is indicated with q while μ denotes the load multiplier.

To apply the numerical procedure the nanobeam axis has been discretized into 100 segments, $\Delta s = \frac{L}{N-1}$, using $N = 101$ sampling nodes. To obtain the first-step trial solution, a small value of the load multiplier is assumed ($\mu = 1$) and the law of bending moment in the linear theory (iteration (1)), for each node $j = 1, 2, \dots, N$ of the domain, is assessed: $m_{x(j)}^{ext(1)} = \frac{\mu q}{2} (L Z_j - Z_j^2)$. With $m_{x(j)}^{ext(1)}$, the corresponding discretized kinematic functions $v_N^{(1)}(Z_j)$, $w_N^{(1)}(Z_j)$ and $\theta_N^{(1)}(Z_j)$ can be evaluated using the discretized forms of equations (24) and (25). Subsequently, the load multiplier is increased (up to $\mu = 10$) and at each iteration (k) the law of the moment, which now depends on the displacements calculated in the previous iteration ($k-1$), is updated. For $q = 0.01$ and $\mu = 10$, the numerical algorithm converges with 50 iterations (in this case, the coincidence with the previous iterative solution to the fourth decimal place is obtained). By this first computation, the local solution ($\varrho = 0$) is achieved. Using the lighter color, the deformed shape of the nanobeam for $\varrho = 0$ is shown in Fig. 4 (this geometric representation is performed to exact scale). As it can be seen, the shape assumed by the axis in this first case is similar to a parabola.

Through (22) it is possible to calculate in each section (that is, at each node j) the longitudinal component of the nonlocal Cauchy stress tensor $T_{3(j)}^{nl}(\rho, \beta)$, conveniently expressed in polar coordinates. The computation of the integral in

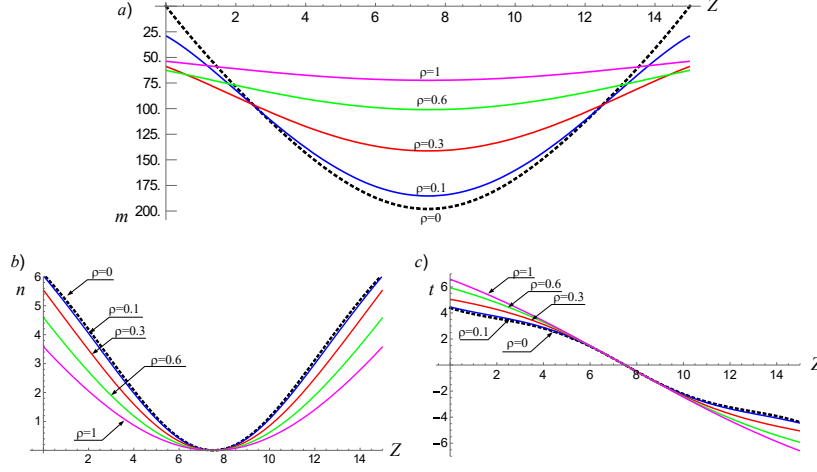


Figure 5: Internal actions. a) Bending moment diagram. b) Normal force diagrams. c) Shear force diagrams.

(22) can be performed using the trapezoidal rule

$$T_{3(j)}^{nl}(\rho, \beta) = \frac{1}{2L_c} \frac{\Delta s}{2} \sum_{n=2}^N \left(e^{-\frac{|Z_j - Z_{n-1}|}{L_c}} T_{3(n-1)}(\rho, \beta) + e^{-\frac{|Z_j - Z_n|}{L_c}} T_{3(n)}(\rho, \beta) \right). \quad (32)$$

With (32) and (23) the internal bending moment $m_x^{int}(Z_j)$ can be determined and then the equilibrium condition (24), together with (25), can be imposed in order to obtain the nonlocal solution. For this purpose, a second iterative procedure is required due to the nonlinearities of (24). Some operational details of such a procedure are described below. Assuming a small value for the parameter ϱ , for example $\varrho = 0.1$, and using (23), with the first attempt values of $\rho_{min}(Z_j)$, $\rho_{max}(Z_j)$ and $\beta_0(Z_j)$ coinciding with those already supplied by the local solution, the moment $m_{x(j)}^{int(1)}$ is evaluated for each node j . By means of (24), (25) and (5) it is then possible to evaluate the discretized kinematic functions $v_N^{(1)}(Z_j)$, $w_N^{(1)}(Z_j)$ and $\theta_N^{(1)}(Z_j)$ and also the longitudinal radius $R^{(1)}(Z_j)$. Based on the values of $R^{(1)}(Z_j)$, the geometrical parameters $\rho_{min}(Z_j)$, $\rho_{max}(Z_j)$ and $\beta_0(Z_j)$ can be updated. Therefore the calculation of (23) is repeated and then the moment-curvature relationship (24) is applied and so on until convergence. Thus the nonlocal solution for $\varrho = 0.1$ is obtained. Twenty iterations are enough to achieve a very good approximation. Starting from the previous solution, the parameter ϱ is increased ($\varrho = 0.2$) and the procedure is repeated. And so on with increments of $\Delta\varrho = 0.1$, up to the final value $\varrho = 1$. All this while keeping the value of the multiplier $\mu = 10$ fixed.

Fig. 4 shows the deflection curves corresponding to the nonlocal solutions for $\varrho = 0.1, 0.3, 0.6$ and 1 . As the nonlocal parameter ϱ increases, it can be seen

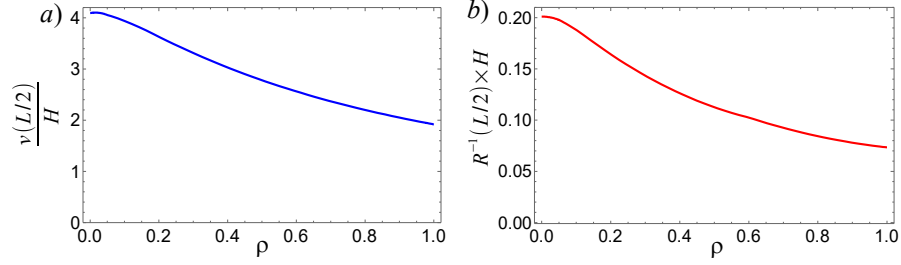


Figure 6: Deformation of the middle cross section. *a)* Deflection. *b)* Curvature.

that the shape of the deflection curve evolves from a parabola-like curve for the local solution to another that tends to approach an arc of circumference for $\varrho = 1$, which is represented with the strongest color. Therefore, the nonlocal effect makes the curvature more uniform along the axis of the nanobeam. In particular, it decreases in the middle while growing near the supports. Obviously, the stresses also decrease in the central portion of the nanobeam as ϱ increases. This can be seen again from Fig. 4, where the vertical profiles of the Cauchy stress for the middle cross section are illustrated.

As ϱ increases, together with the curvature, the bending moment diagram tends to become almost constant, as can be seen in Fig. 5a. Again in the case of increasing ϱ , the diagram of the shear force increases, becoming almost linear for $\varrho = 1$ (cf. Fig. 5c), while the diagram of the normal force decreases (cf. Fig. 5b).

Finally, with reference to the middle cross section, Fig. 6 shows the curvature and the vertical displacement as ϱ varies.

5 Conclusions

The bending theory for nanobeams in the fully nonlinear framework of finite elasticity is presented in this paper. The proposed analysis can be applied to an extensive variety of emerging problems in the modern nanotechnology, for which well-founded equilibrium solutions are lacking in literature.

The kinematics of nanobeams has been modeled according to the classic Navier-Bernoulli hypothesis which prescribes that cross sections deform preserving their planarity. Both deformations and displacements are considered large and the anticlastic deformation of the cross sections has been also taken into account. The developed kinematic model provides the entire three-dimensional displacement field of nanobeams. Extending the Eringen's original idea, a non-local constitutive law in integral form has been defined for the Cauchy stress tensor. Equilibrium has been imposed, for each individual cross section, by equating the internal bending moment, generated by the longitudinal Cauchy stresses, with the external bending moment, generated by the external loads and

evaluated with respect to the deformed nanobeam axis. This latter equilibrium condition plays the role of a moment-curvature relationship in the fully nonlinear context of finite elasticity, since it relates the external bending moment with the longitudinal curvature of the nanobeam axis.

The governance equations take the form of a coupled system of three equations in integral form, which, given its nonlinearities, is solved numerically through an iterative procedure. Indeed, the iterative procedure has to be applied twice. The first time to get the local solution, which is inserted into the second iterative procedure to obtain the nonlocal solution. These numerical computations provide the displacement components and the rotation of each point belonging to the nanobeam axis. Knowing these kinematic functions, the shape assumed by the nanobeam in the deformed configuration as well as the stretches and stresses in every point can be assessed.

All the mathematical formulation was performed for a generic hyperelastic and isotropic material. In view of the applications, the analysis was then specialized for compressible Mooney-Rivlin materials and a simply supported nanobeam under uniformly distributed loads was considered. The effect of nonlocality on longitudinal curvatures and internal action diagrams was shown through some graphs. The results of the nonlocal solution were discussed and compared with those of the local solution.

Acknowledgment

The authors wish to thank professors R. Luciano and F. Marotti of Sciarra for the fruitful discussions on nanobeams. Financial support from the Italian Ministry of Education, University and Research (MIUR) in the framework of the Project PRIN2017 "Modelling of constitutive laws for traditional and innovative building materials" (code 2017HFPKZY) is gratefully acknowledged.

References

- [1] E. Kröner, Elasticity theory of materials with long range cohesive forces. *Int. J. Solids Struct.* **3** (1967) 731–742.
- [2] J.A. Krumhansl, Some Considerations of the Relation between Solid State Physics and Generalized Continuum Mechanics. *Mechanics of Generalized Continua* (1968) 298–311.
- [3] D.G.B. Edelen, N. Laws, On the thermodynamics of systems with nonlocality. *Arch. Ration. Mech. Anal.* **43** (1971) 24–35.
- [4] D.G.B. Edelen, A.E. Green, N. Laws, Nonlocal continuum mechanics. *Arch. Ration. Mech. Anal.* **43** (1971) 36–44.
- [5] A.C. Eringen, D.G.B. Edelen, On nonlocal elasticity. *Inter. J. of Eng. Science* **10** (1972) 233–248.

- [6] A.C. Eringen, B.S. Kim, Stress concentration at the tip of crack. *Mech. Res. Commun.* **1** (1974) 233–237.
- [7] A.C. Eringen, Theory of nonlocal thermoelasticity. *Inter. J. of Eng. Science* **12** (1974) 1063–1077.
- [8] A.C. Eringen, Theory of nonlocal elasticity and some applications. *Res. Mech.* **21** (1987) 313–342.
- [9] J. Peddieson, G.R. Buchanan, R.P. McNitt. Application of nonlocal continuum models to nanotechnology. *Inter. J. of Eng. Science* **41** (3-5) (2003) 305–312.
- [10] G.L. She, F.G. Yuan, B. Karami, Y.R. Ren, W.S. Xiao, On nonlinear bending behavior of FG porous curved nanotubes. *Inter. J. of Eng. Science.* **135** (2019) 58-74.
- [11] M.H. Jalaei, Ö. Civalek, On dynamic instability of magnetically embedded viscoelastic porous FG nanobeam. *Inter. J. of Eng. Science.* **143** (2019) 14-32.
- [12] A. Farajpour, M.H. Ghayesh, H. Farokhi, A review on the mechanics of nanostructures. *Inter. J. of Eng. Science.* **133** (2018) 231-263.
- [13] R. Barretta, M. Čanadija, F. Marotti de Sciarra, On thermomechanics of multilayered beams. *Inter. J. of Eng. Science.* **155** (2020) doi.org/10.1016/j.ijengsci.2020.103364.
- [14] H. Darban, F. Fabbrocino, R. Luciano, Size-dependent linear elastic fracture of nanobeams. *Inter. J. of Eng. Science.* **157** (2020) doi.org/10.1016/j.ijengsci.2020.103381.
- [15] Q. Wang, Y. Liu, Review of optical fiber bending/curvature sensor. *Measurement* **130** (2018) 161-176.
- [16] B. Huang, M. Li, T. Mei, D. McCoul, S. Qin, Z. Zhao, J. Zhao, Wearable Stretch Sensors for Motion Measurement of the Wrist Joint Based on Dielectric Elastomers. *Sensors* **17** (2017) 2708, doi.org/10.3390/s17122708.
- [17] J. Costa, F. Spina, P. Lugoda, L. Garcia, D. Roggen, N. Münzenrieder, Flexible Sensors-From Materials to Applications. *Technologies* **7** (2019) 35, doi:10.3390/technologies7020035.
- [18] Z. Wang, Y. Yao, X. Wang, W. Yue, L. Chen, X. Xiang Zhangb, Bending-induced electromechanical coupling and large piezoelectric response in a micromachined diaphragm. *Sci Rep.* **3** (2013) 3127, doi:10.1038/srep03127.
- [19] G. Wang, M. Shahinpoor, Design, prototyping and computer simulations of a novel large bending actuator made with a shape memory alloy contractile wire. *Smart Mater. Struct.* **6** (1997) 214, doi.org/10.1088/0964-1726/6/2/011.

- [20] L. Qi, S. Huang, G. Fu, S. Zhou, X. Jiang, On the mechanics of curved flexoelectric microbeams. *Inter. J. of Eng. Science.* **124** (2018) 1-15.
- [21] M. Reza Barati, On non-linear vibrations of flexoelectric nanobeams. *Inter. J. of Eng. Science.* **121** (2017) 143-153.
- [22] V.A. Eremeyev, J.F. Ganghoffer, V. Konopińska-Zmysłowska, N.S. Uglov, Flexoelectricity and apparent piezoelectricity of a pantographic micro-bar. *Inter. J. of Eng. Science.* **149** (2020) 103213.
- [23] Q. Liu, H. Zhan, H. Zhu, Z. Sun, J. Bell, A. Bo, Y. Gu, Atomic-scale investigation on the ultra-large bending behaviours of layered sodium titanate nanowires. *Nanoscale* **24** (2019).
- [24] P. Koirala, C.A. Mizzi, L.D. Marks, Direct Observation of Large Flexoelectric Bending at the Nanoscale in Lanthanide Scandates. *Nano Lett.* **18** (2018) 3850-3856.
- [25] F.O. Falope, L. Lanzoni, A. M. Tarantino, The bending of fully nonlinear beams. Theoretical, numerical and experimental analyses. *Inter. J. of Eng. Science.* **145** (2019) 103167.
- [26] L. Lanzoni, A.M. Tarantino, Finite anticlastic bending of hyperelastic solids and beams. *J. Elasticity* **131** (2018) 137-170, doi.org/10.1007/s10659-017-9649-y.
- [27] F.O. Falope, L. Lanzoni, A. M. Tarantino, Bending device and anticlastic surface measurement of solids under large deformations and displacements. *Mech. Res. Comm.* **97** (2019) 52-56.
- [28] A.M. Tarantino, L. Lanzoni, F.O. Falope, *The bending theory of fully non-linear beams*. Springer (2019).
- [29] L. Lanzoni, A.M. Tarantino, The bending of beams in finite elasticity. *J. Elasticity* (2019) doi.org/10.1007/s10659-019-09746-8.
- [30] A.C. Eringen. Linear theory of nonlocal elasticity and dispersion of plane waves. *Inter. J. of Eng. Science* **10** (5) (1972) 425-435.
- [31] A.C. Eringen. On differential equations of nonlocal elasticity and solutions of screw dislocation and surface waves. *J. Appl. Phys.* **54** (9) (1983) 4703-4710.
- [32] L. Lanzoni, A.M. Tarantino, Mechanics of High-Flexible Beams under Live Loads. *J. Elasticity* (2020) doi.org/10.1007/s10659-019-09759-3.
- [33] F.O. Falope, L. Lanzoni, A. M. Tarantino, FE analyses of hyperelastic solids under large bending: The role of the Searle parameter and Eulerian slenderness. Submitted to *Materials MDPI* (2020).

- [34] A.M. Tarantino, Equilibrium paths of a hyperelastic body under progressive damage. *J. Elasticity* **114** (2014) 225-250.
- [35] L. Lanzoni, A.M. Tarantino, Damaged hyperelastic membranes. *Inter. J. Nonlinear Mech.* **60** (2014) 9-22.
- [36] L. Lanzoni, A.M. Tarantino, Equilibrium configurations and stability of a damaged body under uniaxial tractions. *ZAMP J. of Appl. Math. and Phys.* **66** (2015) 171-190.
- [37] J.M. Ciarlet, G. Geymonat, Sur les lois de comportement en élasticité non-linéaire compressible. *C.R. Acad Sci. Paris Sér. II* **295** (1982) 423-426.
- [38] L. Lanzoni, A.M. Tarantino, A simple nonlinear model to simulate the localized necking and neck propagation. *Inter. J. Nonlinear Mech.* **84** (2016) 94-104.
- [39] M. Pelliciari, A.M. Tarantino, Equilibrium paths for Von Mises trusses in finite elasticity. *J. Elasticity* **57** (2019).
- [40] M. Pelliciari, A.M. Tarantino, Equilibrium paths for Von Mises trusses in finite elasticity. *Math. and Mech of Solids* **25** (2020) 705-726.